Icarus 246 (2015) 352–359

Contents lists available at ScienceDirect

Icarus

journal homepage: www.elsevier.com/locate/icarus

Interplanetary dust influx to the Pluto–Charon system

Andrew R. Poppe

Space Sciences Laboratory, 7 Gauss Way, University of California at Berkeley, Berkeley, CA 94720, USA

ARTICLE INFO

Article history:
Available online 15 January 2014

Keywords:
Interplanetary dust
Pluto
Kuiper Belt

ABSTRACT

The influx of interplanetary dust grains (IDPs) to the Pluto–Charon system is expected to drive several physical processes, including the formation of tenuous dusty rings and/or exospheres, the deposition of neutral material in Pluto's atmosphere through ablation, the annealing of surface ices, and the exchange of ejecta between Pluto and its satellites. The characteristics of these physical mechanisms are dependent on the total incoming mass, velocity, variability, and composition of interplanetary dust grains; however, our knowledge of the IDP environment in the Edgeworth-Kuiper Belt has, until recently, remained rather limited. Newly-reported measurements by the New Horizons Student Dust Counter combined with previous Pioneer 10 meteoroid measurements and a dynamical IDP tracing model have improved the characterization of the IDP environment in the outer Solar System, including at Pluto–Charon. Here we report on this modeling and data comparison effort, including a discussion of the IDP influx to Pluto and its moons, and the implications thereof.

1. Introduction

All objects in the Solar System are subject to a flux of submicron to millimeter sized dust grains and knowledge of this influx is critical for understanding several physical processes in the Pluto–Charon system. For example, interplanetary dust flux should drive the production of tenuous dusty rings or exospheres. Modeling efforts have shown that ejecta from Pluto's smaller satellites (Nix and Hydra, as well as the newly-discovered Kerberos and Styx) dominates the equilibrium density of grains within the Pluto–Charon system (Thiessenhusen et al., 2002; Poppe and Horányi, 2011; Pires dos Santos et al., 2013); however, estimates of the expected geometric optical depth of such rings diverge over several orders of magnitude. Observational searches for any rings through either direct backscattering or stellar occultation have yielded no detections and have correspondingly placed an upper limit for the optical depth of approximately 6×10^{-6} at the orbit of Hydra (Steffl and Stern, 2007). Characterizing the interplanetary dust influx to the Pluto system will allow for more accurate calculations of any putative ring densities and optical depths. The presence of impact ejecta within the Pluto–Charon system will contribute to ejecta transfer amongst Pluto and its satellites, mainly from the smaller satellites to larger (Stern, 2009; Poppe and Horányi, 2011), which may be a process by which the albedos and colors of Pluto's satellites may evolve to a self-similar state. Interplanetary dust bombardment may anneal water ice on the surfaces of Charon and the smaller satellites, helping to explain the presence of crystalline water ice in the outer Solar System where it is energetically disfavored over amorphous water ice (Porter et al., 2010). Finally, interplanetary dust bombardment may contribute to other processes not yet considered for the Pluto–Charon system, including the production of neutral exospheres via impact vaporization similar to the Moon and Mercury (Verani et al., 1998; Stern, 1999), the deposition of external material in Pluto's atmosphere via ablation and its subsequent photochemical consequences (Krasnopolsky and Cruikshank, 1999; Krasnopolsky, 2012), and impact gardening of surfaces in the Pluto–Charon system (Papike et al., 1982; Lucey et al., 2006).

At the Pluto–Charon system, the interplanetary dust distribution is dominated by grains produced from the Edgeworth-Kuiper Belt (EKB) itself through both mutual collisions and bombardment of EKB objects by interstellar grains (Stern, 1996; Yamamoto and Mukai, 1998), with a small contribution from cometary sources (Landgraf et al., 2002); however, given the historically limited in situ dust density measurements outside the orbit of Jupiter, dust fluxes in the outer Solar System have often been estimated by using the well-characterized flux at 1 AU (Grün et al., 1985) and extrapolating outwards. Since the Grün et al. (1985) model applies to asteroidal and cometary dust produced within the orbit of Jupiter, it does not necessarily represent the dust complex in the outer Solar System, where the sources and dynamics of IDPs are quite different. Recently reported measurements of dust densities in the outer Solar System by the Student Dust Counter (Horányi et al., 2008; Poppe et al., 2010) onboard the New Horizons mission to Pluto (Stern, 2008), when combined with previous Pioneer 10 meteoroid detector measurements (Humes, 1980) and a dynamical model (Han et al., 2011), are now constraining the interplanetary dust density and velocity distributions in the outer Solar System, from which dust influx distributions can be calculated.

E-mail address: poppe@ssl.berkeley.edu

0019-1035/$ - see front matter © 2014 Elsevier Inc. All rights reserved.
http://dx.doi.org/10.1016/j.icarus.2013.12.029

In this paper, we calculate the magnitude and variability of the interplanetary dust influx to the Pluto–Charon system using a dynamical dust tracing model and in situ dust density measurements by the Pioneer 10 and New Horizons spacecraft. Section 2 describes the dust model and Section 3 presents the influx calculations to the Pluto–Charon system. Finally, we discuss implications and conclude in Sections 4 and 5, respectively.

2. Interplanetary dust model

In order to calculate the interplanetary dust flux to the Pluto–Charon system, we use the results of a dynamical dust grain tracing model described in detail in Han et al. (2011). This code models the behavior of dust grains originating from the Edgeworth-Kuiper Belt for a discrete collection of grain sizes in the range of 0.5–50 μm. Grains are launched with initial conditions corresponding to known EKB sub-populations, namely, classical, scattered, and resonant objects (Kavelaars et al., 2009), although we note that recently reported investigations into the orbital structure of the EKB may affect these results by refining the estimates of the number and distribution of various sub-populations (e.g., Petit et al., 2011; Gladman et al., 2012). Each grain is subject to variety of forces, including solar and outer planetary gravitation, solar radiation pressure, Poynting–Robertson drag, and the electromagnetic interaction with the interplanetary magnetic field (Burns et al., 1979; Gustafson, 1994). All grains are modeled as silicates with density $\rho = 2.5$ g cm^{-3}, although, we note that dust grains with other compositions (i.e., icy or carbonaceous) may exist due to the extensive diversity of surface compositions amongst EKB objects (Brown, 2012). Individual grains are followed until they either reach the far inner Solar System (defined as inside 0.1 AU) or are ejected from the Solar System. The dust grain state vector data are routinely printed out, from which statistical equilibrium maps of the three-dimensional dust grain density and velocity distributions at each grain size can be constructed (Liou and Zook, 1999). At this time, we do not consider interplanetary grain–grain collisions, although, previous modeling work has shown that collisions may play a role in modifying size distributions of EKB grains (Kuchner and Stark, 2010). Additionally, collisions between interstellar grains and interplanetary grains may be an efficient mass-loss mechanism and could alter the equilibrium distribution; however, we neglect this effect presently but identify the inclusion of interstellar grain impacts as a future task. Fig. 1 shows the relative density of 10 μm EKB-generated grains in (a) the ecliptic plane for the Neptune-rotated frame and (b) in the vertical plane where the dust density has been azimuthally averaged. Mean-motion resonances dominate the behavior of dust grains outside the orbit of Neptune, yielding the complex density structure both radially and azimuthally. The character of these structures depends on the dust parent bodies (EKB classical, scattered or resonant objects) as well as the dust grain size and composition. In general, larger grains and/or dynamically colder grains have longer resonance lifetimes with Neptune and thus, have equilibrium density distributions with a higher degree of structure (Liou and Zook, 1999; Moro-Martín and Malhotra, 2003).

To provide an absolute measure of the EKB density throughout the Solar System, the model has been compared to both Pioneer 10 and New Horizons Student Dust Counter (SDC) measurements (Humes, 1980; Horányi et al., 2008; Poppe et al., 2010). Since SDC measures grains larger than approximately 0.5 μm while Pioneer 10 measured grains larger than approximately 3.5 μm, both the overall dust production rate from the EKB and the slope of the corresponding mass distribution have been constrained (Han et al., 2011). The dust production mass distribution is assumed to be in a longitudinally-averaged, quasi-steady state equilibrium

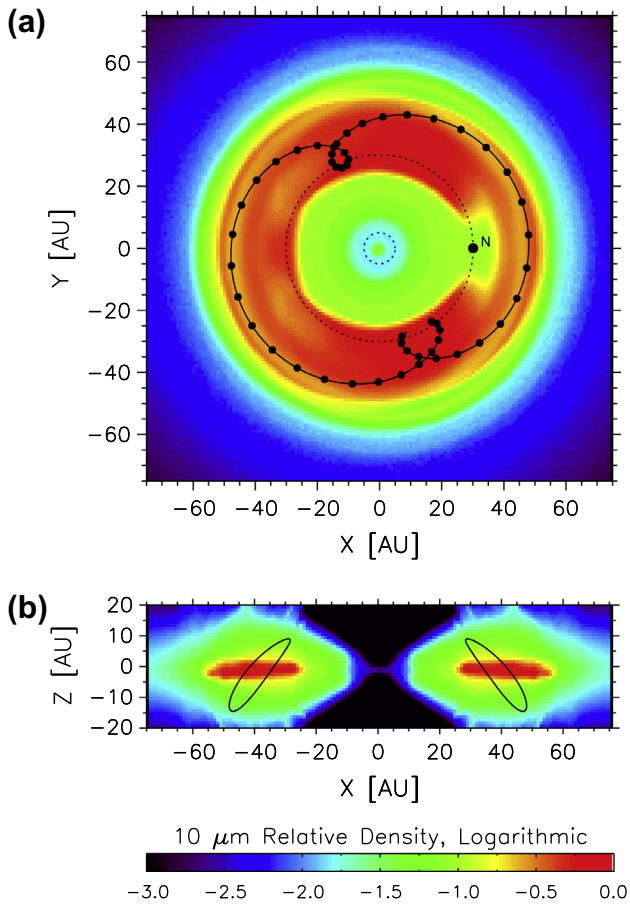

Fig. 1. The equilibrium density of 10 μm Edgeworth-Kuiper Belt grains (a) in the ecliptic, Neptune-rotated frame and (b) in the azimuthally averaged, vertical plane containing the Sun and Neptune. Overplotted on both panels is the orbit of Pluto, also in the Neptune-rotated frame. Additionally, the orbits of Neptune and Jupiter are shown as thin dotted lines.

(based on calculations by Stern (1996) and Yamamoto and Mukai (1998)), that follows a power law given by $d\dot{M}/dm = \dot{M}_o(m/m_o)^{-\alpha/3}$, where $\dot{M}$ is the overall dust production rate, $\dot{M}_o$ is a normalization constant, $m_o = 10^{-11}$ g is a reference grain mass, and $\alpha = 3.02$ is the slope of the mass distribution (Han et al., 2011). The overall mass production rate of dust grains between 0.1 and 10 μm in radius in the EKB was found to be approximately $\dot{M} = 8.9 \times 10^5$ g/s (Han et al., 2011), well within the range estimated theoretically (Stern, 1996; Yamamoto and Mukai, 1998). From these constraints, the density, velocity, and mass distributions of micron-sized EKB grains can be calculated throughout the Solar System.

3. IDP flux to Pluto

Overplotted on both panels of Fig. 1 are projections of the trajectory of the Pluto–Charon system in the Neptune-rotated frame. In Fig. 1(a), where the trajectory is projected onto the ecliptic plane, we see that Pluto (as a Neptune-resonant object itself) orbits through the densest part of the 10 μm EKB grain density. In addition to the variability of the dust density in the ecliptic plane, one must also consider the vertical variation of the EKB dust density above and below the ecliptic plane for the case of the Pluto system. Pluto has an orbital inclination of approximately 17.1° and attains a maximum distance above and below the ecliptic plane of approximately 10 and 15 AU, respectively. The 10 μm EKB dust

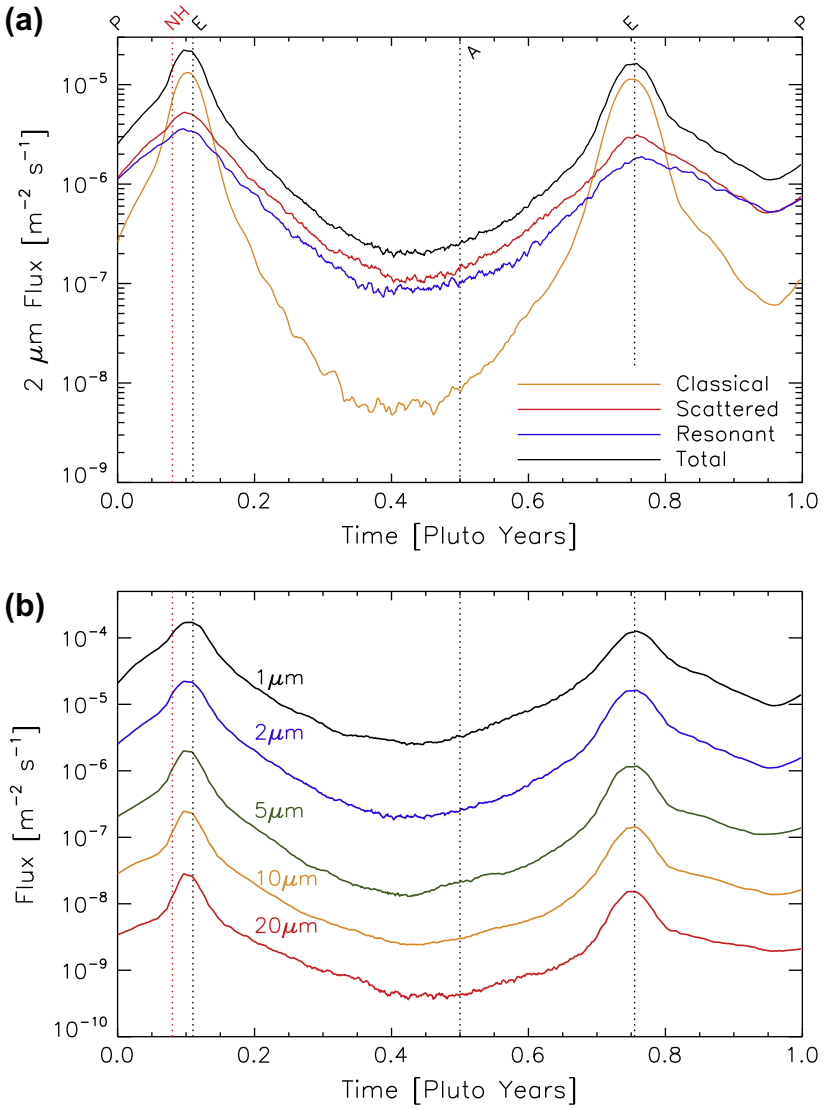

Fig. 2. (a) The flux of classical, scattered, and resonant 2 μm EKB grains to Pluto as a function of time over one Pluto year. (b) The total 0.5, 2, 5, 10, and 20 μm EKB dust flux to Pluto as a function of time over one Pluto year. The perihelion ('P'), aphelion ('A'), ecliptic plane crossings ('E'), and relative time of the New Horizons fly-by ('NH') are marked as dotted vertical lines.

density varies by more than an order of magnitude vertically along Pluto's orbit as shown in Fig. 1(b). To calculate the flux of EKB grains to the Pluto–Charon system along its orbit we followed the method described in Poppe and Horányi (2012) where the EKB dust flux to Saturn was calculated. Briefly, Pluto was traced through the three-dimensional dust distributions for each modeled grain size and the density and velocity were calculated by assuming that grains within 0.5 AU of Pluto impacted the system. Pluto's velocity was vectorially added to the dust grain velocities and in turn, convolved with the local dust grain density to obtain the flux at Pluto's Hill radius (i.e., before any local gravitational acceleration into the Pluto–Charon system). The sole enhancement for this work over our calculations for Saturn is the inclusion of the vertical variability in the EKB dust grain density (critical for Pluto, but not necessarily so for Saturn, which has an orbital inclination of only 2.5°).

Fig. 2(a) shows the flux of 2 μm classical, scattered, and resonant EKB grains, as well as the total 2 μm flux, respectively, to the Pluto–Charon system as a function of time for one Pluto year. Also noted as vertical dotted lines on the plot are Pluto's perihelion ('P'), aphelion ('A'), ecliptic plane crossings ('E'), and the time of the New Horizons fly-by ('NH', in red).[1] The classical EKB influx is variable over more than three orders of magnitude from 10^{-8} to 10^{-5} m^{-2} s^{-1}. This variability is due to the concentration of the classical EKB grains in the ecliptic plane due to the dynamically cold nature of the parent classical EKB objects. As the Pluto–Charon system passes through the ecliptic plane on its inclined orbit (both ascending and descending), the classical EKB flux increases dramatically and at its highest level is the dominant influx to Pluto (over the scattered and resonant components). Relative to a Pluto year, this peak is brief, occurring within just 15 (Earth) years (defined as the classical flux being above the full-width half-max). In contrast, the hotter dynamical nature of the scattered and resonant EKB objects yields a dust complex that has higher eccentricities and inclinations and thus, the scattered and resonant dust grain densities extend to higher ecliptic latitudes relative to the classical component. In turn, the scattered and resonant grain fluxes to Pluto drop less dramatically

[1] For interpretation of color in Figs. 2 and 3, the reader is referred to the web version of this article.

than the classical component, roughly a factor of 50 (by itself still significant). In total, the 2 μm flux to Pluto varies by approximately two orders of magnitude over its year. Fig. 2(b) shows the EKB flux to Pluto for five different grain sizes: 0.5, 2, 5, 10, and 20 μm, each summed over their respective classical, scattered, and resonant components. As expected, the overall magnitude of the flux decreases as the grain size increases, yet nearly identical variability is seen in all grain sizes over the course of one Pluto year.

Having calculated the flux of EKB grains to Pluto as a function of time and grain size, we naturally wish to compare with previous methods of estimating the dust flux to Pluto. Such an estimate is typically obtained by taking the dust flux at 1 AU as described by Grün et al. (1985) and extrapolating out to the heliocentric distance of Pluto by: (1) assuming that the spatial density of interplanetary dust grains remains constant since the Pioneer 10 meteoroid detector measured a near-constant flux of ≈3.5 μm grains outside the orbit of Jupiter (Humes, 1980), and (2) re-computing the impact velocity to take into account the slower heliocentric velocities at Pluto. Fig. 3(a) shows a comparison of the Grün et al. (1985) differential number flux extrapolated to 30 AU as a function of grain size and the differential number flux from this model at its highest (blue) and lowest (red) values. For grain sizes larger than those that we simulated (> 50 μm), we show two possible extensions for the differential flux. The dashed lines in each case represent a simple power-law extrapolation of the modeled flux out to 10^4 μm. In contrast, the continuing solid line uses the slope of the Grün et al. (1985) flux for radii greater than 50 μm appropriately normalized to match the differential flux for both the minimum and maximum cases modeled here. We suspect that the Grün et al. (1985) extrapolation may be more physically correct due to the effect of grain–grain collisions on the size distribution, which will tend to remove mass from the larger sizes and redistribute them to smaller sizes. Grün et al. (1985) have shown that at 1 AU the critical size where collisional gain transitions to collisional loss occurs around 10^{-5} g, or roughly 50–100 μm. To estimate this critical size for the EKB, we compared the lifetimes for Poynting–Robertson drag and collisional destruction in the Edgeworth-Kuiper Belt. Poynting–Roberston drag lifetime expressed in years is taken from Eq. (20) of Grün et al. (1985)

$$T_{PR} = 7 \times 10^6 s \rho Q_{eff} a_o^2 (1 - e_o)^2 E(e_o), \quad (1)$$

where s is the grain radius in cm, ρ is the grain density in g/cm^3, $Q_{eff} = 1$ is the fraction of incident photon momentum absorbed by

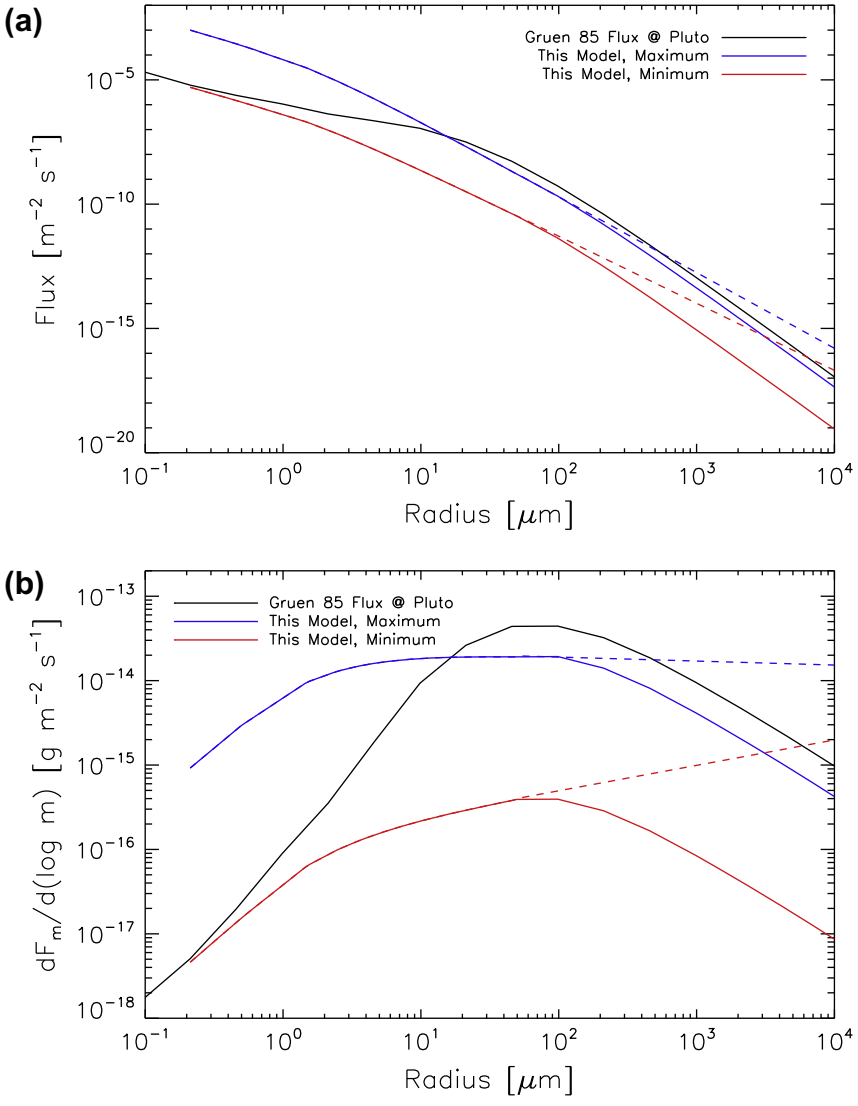

Fig. 3. (a) The differential number flux of EKB dust to Pluto as a function of radius for this model at maximum, this model at minimum, and the extrapolated Grün et al. (1985) flux. The simulated size range from this model is represented by the solid lines, while a linear extrapolation is shown as the dashed line in both cases. (b) The differential mass flux of EKB dust to Pluto as a function of radius (in units of differential mass flux per decade mass) in the same format as (a).

each grain (valid for $m > 10^{-12}$ g), a_o and e_o are the average initial semi-major axis and eccentricity, respectively, and $E(e_o)$ is an empirical function from Wyatt and Whipple (1950). From our dynamical simulations, we use $a_o = 45$ AU and $e_o = 0.25$ for average initial values. The collisional lifetime can be approximated following Kuchner and Stark (2010), who used an expression from Wyatt (2003),

$$T_{coll} = T_{orbit}/(4\pi\tau), \quad (2)$$

where T_{orbit} is a typical orbital period for a grain in the EKB and τ is the face-on optical depth of the EKB. Calculating the orbital period for a grain at 45 AU and using an estimated optical depth of $\tau \approx 10^{-7}$ (Stern, 1996; Yamamoto and Mukai, 1998), we find a collisional lifetime of approximately $T_{coll} = 2 \times 10^8$ yrs. Setting this time equal to the expression for the Poynting–Robertson drag lifetime and solving for the critical radius yields $s \approx 75$ μm. We note that this is slightly higher than the critical radius found by Kuchner and Stark (2010) of approximately 20 μm for the EKB, yet still provides a reasonable estimate for the point at which to "break" the power law. While we have not employed a completely self-consistent treatment of collisions in the EKB dust disk, the extrapolation of the mass distribution using the slope of the Grün et al. (1985) curve is a reasonable estimate for fluxes greater than we have directly modeled. Future models incorporating such effects (c.f. Stark and Kuchner, 2009; Kuchner and Stark, 2010) will allow a more detailed analysis of the flux at Pluto for larger grain sizes. Comparing our modeled curves with Grün et al. (1985) at Pluto, we see that our modeled flux disagrees with the extrapolated Grün et al. (1985) flux both in magnitude and slope. At maximum (blue curve), our model predicts more flux for $a < 15$ μm grains and less flux for $a > 15$ μm grains relative to the extrapolated flux; at minimum (red curve), our model predicts less flux to the Pluto–Charon system for all grain sizes.

In Fig. 3(b) we compare the differential mass influx as a function of logarithmic mass, $dF_m/d(\log m)$ between the extrapolated Grün et al. (1985) model and our model. The Grün et al. (1985) mass flux peaks at approximately 50–100 μm while our model peaks and is flat between 10 and 50 μm at maximum (blue curve), before decreasing under the extrapolation of the Grün et al. (1985)-like slope for larger masses. At minimum (red curve), the mass flux peaks closer to 50 μm, although the overall magnitude of the differential mass flux at minimum is several orders-of-magnitude less than the extrapolated Grün et al. (1985) mass flux. Assuming that the extrapolation of our model holds over grain sizes between 0.1 and 10^4 μm, integrating under the various curves provides the total mass flux to the Pluto–Charon system, listed in Table 1. The extrapolated Grün et al. (1985) model predicts a total mass flux of approximately 1.8×10^{-13} g m^{-2} s^{-1} while the maximum and minimum mass fluxes from this model are approximately 1.4×10^{-13} and 2.1×10^{-15} g m^{-2} s^{-1}, respectively. The mass flux at maximum (during the ecliptic plane crossing) is nearly that of the extrapolated Grün et al. (1985) flux while in contrast, the mass flux at minimum is almost two orders-of-magnitude lower than Grün et al. (1985). Additionally, for further comparison, we also list the interstellar mass flux of 5×10^{-17} g m^{-2} s^{-1} (Grün et al., 1994), which is roughly an additional factor of forty less than the minimum interplanetary flux.

Table 1
A comparison of the total IDP mass influx to the Pluto–Charon system derived from Grün et al. (1985) and this work. Additionally, the mass flux of interstellar dust grains is also listed (Grün et al., 1994).

Source	Total mass flux (10^{-13} g m^{-2} s^{-1})
Grün et al. (1985) at 30 AU	1.8
EKB (this model), maximum	1.4
EKB (this model), minimum	0.021
Interstellar dust	0.0005

4. Implications

The improved model for the influx of interplanetary dust grains to the Pluto–Charon system has several implications for various physical processes. We briefly discuss some of these implications here, with the understanding that to some degree, the Pluto–Charon system serves as an example for EKBOs as a whole and that there remains much work to be done regarding the impact of interplanetary dust bombardment in the Edgeworth-Kuiper Belt. The fly-by of the New Horizons spacecraft past the Pluto–Charon system in mid-2015 will provide a wealth of new observations to compare to the theoretical investigations outlined below.

4.1. Pluto–Charon rings/tori

The influx of interplanetary dust grains is expected to drive many phenomena in the Pluto–Charon system, chief among these the possible production of dust rings or tori comprised of ejecta produced upon IDP impact (Thiessenhusen et al., 2002; Poppe and Horányi, 2011; Pires dos Santos et al., 2013). In Poppe and Horányi (2011), we presented the results of a model of the putative Pluto–Charon dust rings. The overall density and geometric optical depth of any possible ring system is a function of both the typical grain lifetime within the Pluto–Charon system and the total amount of incoming IDP mass flux. Using the extrapolated Grün et al. (1985) mass flux at Pluto of 2.4×10^{-13} g m^{-2} s^{-1} (before any local gravitational acceleration), we predicted a maximum geometric optical depth for 50 μm grains in the Pluto–Charon system of $\tau_{50} = 5 \times 10^{-7}$. Relative to the estimated mass flux from the Grün et al. (1985) extrapolation, the mass flux at the time of the New Horizons fly-by as calculated from our updated EKB dust model is approximately a factor of two lower; however, we must also account for the fact that the dust model presented in Poppe and Horányi (2011) was conducted before the discovery of Styx and Kerberos. The very small size of these two satellites, roughly 10 and 14 km, respectively (Showalter et al., 2011, 2012), implies that they should yield ejecta into the Pluto–Charon system at fluxes roughly equal to Nix and Hydra. The lower incoming dust mass flux and the anticipated contribution of Styx and Kerberos roughly cancel each other out, and thus our estimate for the maximum optical depth for 50 μm grains remains at $\tau_{50} \approx 5 \times 10^{-7}$.

Observations of the Pluto–Charon system during the New Horizons fly-by in July 2015 will search for signatures of dusty rings. The LOng-Range Reconnaisance Imager (LORRI) on New Horizons (Cheng et al., 2008) will thoroughly image the Pluto–Charon system both on the approach and departure phases. For the approach phase, any rings would be detected through backscattering. The minimum I/F brightness detectable by LORRI on approach is approximately 10^{-7} (H. Weaver, priv. comm., 2013). If we assume a particle albedo of $p_v = 0.35$ (taken from the albedo of Pluto's small satellites), our model suggests a backscattered brightness of $I/F \approx 9 \times 10^{-8}$, just below the anticipated background level for LORRI. The smaller sized grains have even lower backscattered I/F given their smaller optical depths. The best opportunity for ring detection will certainly be after closest approach, when any dust rings will forward scatter light at brightnesses at least several times that in backscattered light. If such rings are detected, a detailed comparison of the size and spatial distribution of the rings will help to confirm the models of dust ring production at Pluto–Charon and will extend our confidence in predicting the presence of rings at other Edgeworth-Kuiper Belt objects.

4.2. Micrometeoroid annealing of Charon's icy surface

The influx of interplanetary grains to the Pluto–Charon system also has implications for the icy surface of Charon (and potentially the smaller satellites in the Pluto–Charon system), which shows the presence of crystalline water ice (via the diagnostic 1.65 μm spectral feature (Cook et al., 2007; Mastrapa et al., 2009)). In the outer Solar System, where surface temperatures fall well below 150 K, the formation of amorphous solid water (ASW) is heavily favored over the formation of crystalline water ice. An external heat source must therefore exist to convert ASW into a crystalline form (Jenniskens and Blake, 1996). Impacts from interplanetary dust grains can be a source of heat for this process and calculations have suggested that this process can provide enough external heat to anneal surface ice at the satellites of the outer planets (Porter et al., 2010). It was further suggested that this process should operate in the EKB and would potentially explain several observations of crystalline water ice at various EKBOs (Jewitt and Luu, 2004; Cook et al., 2007; Trujillo et al., 2007; Barkume et al., 2008). For Charon, Porter et al. (2010) calculated minimum IDP mass fluxes of 1.8×10^{-14} and 5×10^{-16} g m^{-2} s^{-1} in order to provide a 20% annealed fraction of surface water ice against the amorphization processes of UV and galactic cosmic ray (GCR) irradiation, respectively, noting that Mastrapa et al. (2009) have shown that a 20% annealed fraction is sufficient to make the icy surface appear nearly fully crystalline. Fig. 4(a) shows the time variation of the total mass influx to Pluto from our EKB dust disk model presented here which tracks the variation in flux shown in Fig. 2. Additionally, the amorphization limits from Porter et al. (2010) are shown as dotted lines. The interplanetary dust mass flux varies above and below the required value for providing a 20% annealing fraction against UV amorphization; however, the mean IDP flux (which is a valid representation of the mass flux since variations in the dust flux over a single orbital period of Pluto of approximately 250 years occur more rapidly than the UV or GCR amorphization timescales of 40 and 1500 kyr, respectively (Cook et al., 2007)) is approximately 1.9×10^{-14} g m^{-2} s^{-1}, nearly exactly at the level required. Thus, IDP bombardment may be responsible for the presence of crystalline water ice on Charon's surface. We note that EKBOs in other sub-populations (e.g., classical, scattered, etc.) will experience different levels of IDP bombardment and thus, as a further test for the effectiveness of ice annealing by micrometeoroid bombardment,

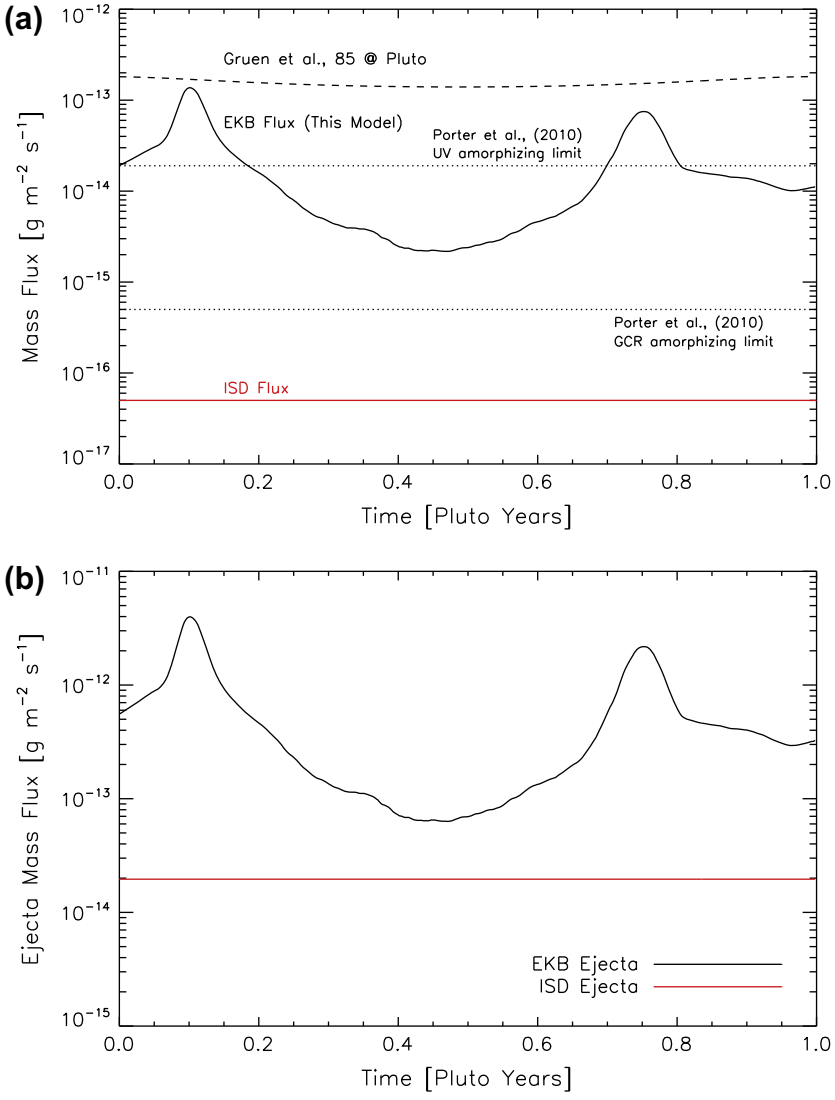

Fig. 4. The (a) incoming mass flux and (b) ejecta mass flux from the Pluto–Charon system as a function of time over Pluto's year from EKB impacts and ISD impacts, respectively. Also shown in (a) are the extrapolated Grün et al. (1985) mass flux (dashed line) and the mass fluxes required to generated a 20% annealed surface ice fraction against UV and GCR amorphization (Porter et al., 2010).

one could search for correlations between IDP flux and crystalline water ice fractions. Finally, while not considered in Porter et al. (2010), interstellar dust bombardment should add additional heat flux to the surfaces of Charon (and other icy satellites or EKBOs), mainly due to the higher kinetic energy of ISD grains due to their much higher impact speeds (>26 km/s) despite the lower ISD mass flux.

4.3. Comparison with interstellar mass flux and generation of the EKB dust disk

In addition to generating grains within the Pluto–Charon system, EKB dust grain bombardment should also produce grains that escape the Pluto–Charon system (either directly, or after a close encounter with one of the satellites within the Pluto–Charon system). Grains that escape become part of the EKB dust complex itself, and represent a mechanism by which the EKB dust complex can "self-generate". This is in addition to the two previously proposed EKB dust grain production methods: mutual EKBO collisions (Stern, 1996) and bombardment of EKBOs by the interstellar dust stream (Yamamoto and Mukai, 1998). While consideration of the former method is beyond the scope of this paper, we can compare production rates of EKB self-generation with ISD bombardment. The total ejecta mass flux for each generation mechanism is a product of the incoming mass flux, Γ_m, and the ejecta yield, Y, for each dust species. To calculate the yield, we use the experimental work of Koschny and Grün (2001), which gives the ejecta yield as a function of impactor mass, m, and speed, v_p, and the silicate surface percentage, G, of the target, as:

$$Y = V_{1,0} \cdot \left(\frac{V_{1,100}}{V_{1,0}}\right)^{G/100} \cdot \left(\frac{1 - G/100}{\rho_{ice}} + \frac{G/100}{\rho_{sil}}\right) \cdot 2^{-b} m_p^{b-1} v_p^{2b}, \quad (3)$$

where ρ_{ice} and ρ_{sil} are the density of ice and silicate, respectively, and $V_{1,0} = 6.69 \times 10^{-8}$ m^3/J, $V_{1,100} = 1.00 \times 10^{-9}$ m^3/J, and $b = 1.23$ are empirically derived constants. For EKB grains, the differential mass flux (Fig. 3(b)) peaks near an impactor mass of 10^{-7} g with impact velocities of ≈3–4 km/s using the EKB dust model including gravitational acceleration from the Pluto–Charon system itself. For interstellar grains, the mean impactor mass and speed are approximately 10^{-14} g and 26 km/s, respectively (neglecting both the small orbital velocity contribution from the Pluto–Charon system as it orbits up- and down-stream with respect to the ISD flow and the gravitational acceleration from the Pluto–Charon system) (Grün et al., 1994; Landgraf et al., 2000). For this exercise, we use $G = 25$ denoting a 75% surface water ice contribution typical of Charon (Brown, 2012), while noting the broad diversity of surface compositions elsewhere in the Edgeworth-Kuiper Belt (Dalton et al., 2010; Brown, 2012). (We note that changing G does not change the relative contributions between EKB and ISD generated ejecta, only the overall magnitude). Using these values, we calculate mass ejecta yields of 30 and 400 for EKB and ISD bombardment, respectively. Convolving this yield with the incoming mass flux for both EKB and ISD grains yields the ejecta mass flux. Fig. 4(a) and (b) show the incoming mass flux and ejecta mass flux, respectively, as a function of time over Pluto's year. The ISD-generated ejecta mass flux is constant throughout Pluto's year at approximately 2×10^{-14} g m^{-2} s^{-1}, while the EKB-generated ejecta mass flux varies between approximately 6.2×10^{-14} and 4.1×10^{-12} g m^{-2} s^{-1}. At Pluto–Charon, EKB-generated ejecta fluxes are greater than the ISD-generated ejecta fluxes over all of Pluto's year, including their maximum, where the EKB-generated ejecta flux is more than two orders of magnitude greater than ISD-generated ejecta.

This example thus prompts the question: Over the entire Edgeworth-Kuiper Belt, which process dominates the generation of EKB dust grains, bombardment by interstellar grains as proposed by Yamamoto and Mukai (1998) or the "self-generation" mechanism proposed here? To answer this, one must solve for the EKB dust fluxes to all EKB objects in a self-consistent manner, taking into account the orbital trajectories of different families of EKBOs. For example, cold classical EKBOs (e.g., the "kernel" population as described by Petit et al. (2011)), which have very low eccentricities and inclinations and semi-major axes centered near 44 AU, are confined to the dense regions of the EKB dust complex and thus, will likely be dominated by EKB-generated ejecta. In contrast, dynamically hotter sub-populations of the EKB (e.g., the scattered disk), will experience variability similar to that shown in the example here for Pluto–Charon, where ecliptic plane crossings are accompanied by high EKB-generated ejecta and periods far from the ecliptic plane or the main EKB dust belt have closer contributions between EKB and ISD generated ejecta. A self-consistent model of EKB dust grain production that takes into account both EKB and ISD dust grain bombardment is beyond the scope of the work presented here, but is identified as a worthy future investigation. An accurate knowledge of dust grain production mechanisms is critical for understanding not only our debris disk, but for the plethora of observed dusty debris disks at other stars (e.g., Greaves et al., 1998; Trilling et al., 2008; Backman et al., 2009; Koerner et al., 2010; Moro-Martín et al., 2010).

5. Conclusion

A dynamical dust grain model constrained by Pioneer 10 and New Horizons Student Dust Counter measurements has been used to calculate the interplanetary dust flux to the Pluto–Charon system. Due to the concentration of the EKB dust disk in the plane of the ecliptic and Pluto's inclined orbit ($i \approx 17^\circ$), the dust flux to the Pluto–Charon system varies over one order-of-magnitude in number flux and more than two orders-of-magnitude in mass flux. The peak "dust seasons" at Pluto are during ecliptic crossings while the dust flux minima occur near aphelion and just prior to perihelion, corresponding the Pluto's maximum vertical extent either above or below the ecliptic plane. The net mass flux to the Pluto–Charon system ranges between 2.1×10^{-15} and 1.4×10^{-13} g m^{-2} s^{-1}, less than that predicted by extrapolating the Grün et al. (1985) model out to the orbit of Pluto. We have addressed several of the implications of this dust flux and its variability to the Pluto–Charon system, yet note that observations by the New Horizons spacecraft in mid-2015 will shed significant light on several of these processes. Additionally, the model presented here can be used to study further phenomena of interest at the Pluto–Charon system, including meteoritic ablation in Pluto's N_2 atmosphere and its subsequent photochemical consequences (Krasnopolsky, 2012) and the production of neutral exospheres at Charon and the smaller satellites via meteoroid bombardment, for example. Importantly, continued observations by the Student Dust Counter (Horányi et al., 2008; Szalay et al., 2013) throughout the entire EKB dust disk will help to further constrain the distribution of dust grains and their subsequent flux to EKBOs. Finally, we note that while Pluto and its satellites are unique in many ways, they nonetheless serve as an archetypical example of ways in which interplanetary dust influx can drive or influence basic planetary processes at Edgeworth-Kuiper Belt objects. As exploration of the Edgeworth-Kuiper Belt continues, we look forward to drawing important analogues between the Pluto–Charon system and its brethren.

Acknowledgments

The author gratefully acknowledges support from NASA's Planetary Atmospheres Program, Grant #NNX13AG55G. The author

also acknowledges useful comments from H. Weaver, M. Horányi, J. Szalay, and two anonymous reviewers.

References

Backman, D. et al., 2009. Epsilon Eridani's planetary debris disk: Structure and dynamics based on spitzer and caltech submillimeter observatory observations. Astrophys. J. 690, 1522–1538.

Barkume, K.M., Brown, M.E., Schaller, E.L., 2008. Near-infrared spectra of Centaurs and Kuiper Belt Objects. Astron. J. 135, 55–67.

Brown, M.E., 2012. The compositions of Kuiper Belt Objects. Annu. Rev. Earth Planet. Sci. 40, 467–494.

Burns, J.A., Lamy, P.L., Soter, S., 1979. Radiation forces on small particles in the Solar System. Icarus 40, 1–48.

Cheng, A.F. et al., 2008. Long-range reconnaissance imager on new horizons. Space Sci. Rev. 140, 189–216.

Cook, J.C., Desch, S.J., Roush, T.L., Trujillo, C.A., Geballe, T.R., 2007. Near-infrared spectroscopy of Charon: Possible evidence for cryovolcanism on Kuiper Belt Objects. Astrophys. J. 663, 1406–1419.

Dalton, J.B. et al., 2010. Chemical composition of icy satellite surfaces. Space Sci. Rev. 153, 113–154.

Gladman, B. et al., 2012. The resonant trans-Neptunian populations. Astron. J. 144 (23), 1–24.

Greaves, J.S. et al., 1998. A dust ring around epsilon Eridani: Analog to the young Solar System. Astrophys. J. 506, L133–L137.

Grün, E., Zook, H.A., Fechtig, H., Giese, R.H., 1985. Collisional balance of the meteoric complex. Icarus 62, 244–272.

Grün, E. et al., 1994. Interstellar dust in the heliosphere. Astron. Astrophys. 286, 915–924.

Gustafson, B.A.S., 1994. Physics of zodiacal dust. Annu. Rev. Earth Planet. Sci. 22, 553–595.

Han, D., Poppe, A.R., Piquette, M., Grün, E., Horányi, M., 2011. Constraints on dust production in the Edgeworth-Kuiper Belt from Pioneer 10 and New Horizons measurement. Geophys. Res. Lett. 38, L24102.

Horányi, M. et al., 2008. The student dust counter on the new horizons mission. Space Sci. Rev. 140, 387–402.

Humes, D.H., 1980. Results of Pioneer 10 and 11 meteoroid experiments: Interplanetary and near-Saturn. J. Geophys. Res. 85 (A11), 5841–5852.

Jenniskens, P., Blake, D.F., 1996. Crystallization of amorphous water ice in the Solar System. Astrophys. J. 473, 1104–1113.

Jewitt, D.C., Luu, J.X., 2004. Crystalline water ice on the Kuiper belt object (50000) Quaoar. Nature 432, 731–733.

Kavelaars, J.J. et al., 2009. The Canada–France Ecliptic Plane Survey – L3 Data Release: The orbital structure of the Kuiper Belt. Astron. J. 137, 4917–4935.

Koerner, D.W. et al., 2010. New Debris Disk Candidates around 49 Nearby Stars. Astrophys. J. 710, L26–L29.

Koschny, D., Grün, E., 2001. Impacts into ice-silicate mixtures: Crater morphologies, volumes, depth-to-diameter ratios, and yield. Icarus 154, 391–401.

Krasnopolsky, V.A., 2012. Titan's photochemical model: Further update, oxygen species, and comparison with Triton and Pluto. Planet. Space Sci. 73, 318–326.

Krasnopolsky, V.A., Cruikshank, D.P., 1999. Photochemistry of Pluto's atmosphere and ionosphere near perihelion. J. Geophys. Res. 104 (E9), 21979–21996.

Kuchner, M.J., Stark, C.C., 2010. Collisional grooming models of the Kuiper Belt dust cloud. Astron. J. 140, 1007–1019.

Landgraf, M., Baggaley, W.J., Grün, E., Krüger, H., Linkert, G., 2000. Aspects of the mass distribution of interstellar dust grains in the Solar System from in situ measurements. J. Geophys. Res. 105 (A5), 10,343–10,352.

Landgraf, M., Liou, J.-C., Zook, H.A., Grün, E., 2002. Origins of Solar System dust beyond Jupiter. Astron. J. 123, 2857–2861.

Liou, J.-C., Zook, H.A., 1999. Signatures of the giant planets imprinted on the Edgeworth-Kuiper Belt dust disk. Astron. J. 118 (July), 580–590.

Lucey, P. et al., 2006. Understanding the lunar surface and space–moon interactions. Rev. Min. Geochem. 60, 83–219.

Mastrapa, R.M., Sandford, S.A., Roush, T.L., Cruikshank, D.P., Dalle Ore, C.M., 2009. Optical constants of amorphous and crystalline H_2O–ice: 2.5–22 μm (4000–455 cm^{-1}) optical constants of H_2O–ice. Astrophys. J. 701, 1347–1356.

Moro-Martín, A., Malhotra, R., 2003. Dynamical models of Kuiper Belt dust in the inner and outer Solar System. Astrophys. J. 125, 2255–2265.

Moro-Martín, A. et al., 2010. Locating planetesimal belts in the multiple-planet systems HD 128311, HD 202206, HD 82943 and HR 8799. Astrophys. J. 717, 1123–1139.

Papike, J.J., Simon, S.B., Laul, J.C., 1982. The lunar regolith: Chemistry, mineralogy, and petrology. Rev. Geophys. Space Phys. 20 (4), 761–826.

Petit, J. et al., 2011. The Canada–France Ecliptic Plane Survey – full data release: The orbital structure of the Kuiper Belt. Astron. J. 142.

Pires dos Santos, P.M., Winter, S.M.G., Sfair, R., Mourão, D.C., 2013. Small particles in Pluto's environment: Effects of the solar radiation pressure. Mon. Not. R. Astron. Soc. 430 (4), 2761–2767.

Poppe, A., Horányi, M., 2011. The effect of Nix and Hydra on the putative Pluto–Charon dust cloud. Planet. Space Sci. 59, 1647–1653.

Poppe, A.R., Horányi, M., 2012. On the Edgeworth-Kuiper Belt dust flux to Saturn. Geophys. Res. Lett. 39, L15104.

Poppe, A., James, D., Jacobsmeyer, B., Horányi, M., 2010. First results from the Venetia Burney Student Dust Counter on the New Horizons mission. Geophys. Res. Lett. 37, L11101.

Porter, S.B., Desch, S.J., Cook, J.C., 2010. Micrometeorite impact annealing of ice in the outer Solar System. Icarus 208, 492–498.

Showalter, M.R., Weaver, H.A., Stern, S.A., Steffl, A.J., Young, L.A., 2011. New Satellite of (134340) Pluto: S/2011 (134340) 1. IAU Circular 9221.

Showalter, M.R. et al., 2012. New satellite of (134340) Pluto: S/2012 (134340) 1. IAU Circular 9253.

Stark, C.C., Kuchner, M.J., 2009. A new algorithm for self-consistent three-dimensional modeling of collisions in dust debris disks. Astrophys. J. 707, 543–553.

Steffl, A.J., Stern, S.A., 2007. First constraints on rings in the Pluto system. Astron. J. 133, 1485–1489.

Stern, S.A., 1996. Signatures of collisions in the Kuiper disk. Astron. Astrophys. 310, 999–1010.

Stern, S.A., 1999. The lunar atmosphere: History, status, current problems, and context. Rev. Geophys. 37 (4), 453–491.

Stern, S.A., 2008. The new horizons Pluto Kuiper Belt Mission: An overview with historical context. Space Sci. Rev. 140, 3–21.

Stern, S.A., 2009. Ejecta exchange and satellite color evolution in the Pluto system, with implications for KBOs and asteroids with satellites. Icarus 199, 571–573.

Szalay, J.R., Piquette, M., Horányi, M., 2013. The Student Dust Counter: Status report at 23 AU. Earth Planets Space 65, 1145–1149.

Thiessenhusen, K.-U., Krivov, A.V., Krüger, H., Grün, E., 2002. A dust cloud around Pluto and Charon. Planet. Space Sci. 50, 79–87.

Trilling, D.E. et al., 2008. Debris disks around Sun-like stars. Astrophys. J. 674, 1086–1105.

Trujillo, C.A., Brown, M.E., Barkume, K.M., Schaller, E.L., Rabinowitz, D.L., 2007. The surface of 2003 EL_{61} in the near infrared. Astrophys. J. 655, 1172–1178.

Verani, S., Barbieri, C., Benn, C., Cremonese, G., 1998. Possible detection of meteor stream effects on the lunar sodium atmosphere. Planet. Space Sci. 46 (8), 1003–1006.

Wyatt, M.C., 2003. Resonant trapping of planetesimals by planet migration: Debris disk clumps and Vega's similarity to the Solar System. Astrophys. J. 598, 1321–1340.

Wyatt, S.P., Whipple, F.L., 1950. The Poynting–Robertson effect on meteor orbits. Astrophys. J. 111, 134–141.

Yamamoto, S., Mukai, T., 1998. Dust production by impacts of interstellar dust on Edgeworth-Kuiper Belt objects. Astron. Astrophys. 329, 785–791.